

# Fabrication of nonlinear optical devices in ionically self-assembled monolayers

**Aruna Kroetch**

**Stephen C. Buswell**

**Stephane Evoy**

University of Alberta

Department of Electrical and Computer Engineering  
and

National Institute for Nanotechnology

Edmonton, Alberta, T6G 2V4

Canada

E-mail: evoy@ece.ualberta.ca

**Cemil Durak**

**J. Randy Heflin**

Virginia Polytechnic Institute & State University

Department of Physics

Blacksburg, Virginia 24061

**Vladimir Kochergin**

**Roger Duncan**

Luna Innovations Inc.

3157 State Street

Blacksburg, Virginia 24060

**Abstract.** The development of both “soft” and “hard” fabrication techniques for the patterning of nonlinear photonic devices in ionically self-assembled monolayer (ISAM) films is reported. A combination of electron beam lithography and reactive ion etching was used to pattern two-dimensional holes with a lattice of 710 nm and diameters ranging from 550 to 650 nm. A soft alternative to this fabrication was also demonstrated. Nanoimprint lithography was successfully employed to pattern similar photonic structures with average hole diameters of 490 nm and a lattice spacing of 750 nm, as well as Bragg gratings with a period of 620 nm. Potential impact of this fabrication process on the chemical composition and nonlinear properties of the ISAM films was assessed using Fourier transform infrared spectroscopy, x-ray photoelectron spectroscopy, and second harmonic generation. The spectroscopy techniques confirmed that the chemical composition and bonding of the ISAM films was not adversely affected by the thermal cycles required for nanoimprinting. Second harmonic generation analysis also confirmed that the nanoimprinting process did not affect the nonlinear properties of the material, PCBS/PAH ISAM films, further indicating the suitability of such materials for the nanoimprinting of nonlinear optical photonic structures. © 2009 Society of Photo-Optical Instrumentation Engineers. [DOI: 10.1117/1.3066521]

Subject terms: ionically self-assembled monolayers; nanoimprint lithography; nonlinear optical materials; photonic crystals.

Paper 08069R received Jul. 16, 2008; revised manuscript received Nov. 5, 2008; accepted for publication Nov. 21, 2008; published online Mar. 4, 2009.

## 1 Introduction

There is a sustained interest toward the development of high-quality and robust optical components that would enable the further integration of photonic systems. Photonic crystals offer a promising platform for the manipulation of light compared to traditional methods relying on total internal reflection.<sup>1</sup> By circumventing index contrast confinement, active and passive devices based on photonic crystals could be more compactly designed. Most reports to that effect have, however, been limited to “passive” structures. A photonic crystal technology leveraging nonlinear optical (NLO) materials would augment such platforms by including active devices such as switches and interferometers. Inorganic crystals, such as lithium niobate, are commonly used for such purposes. The materials are, however, costly and difficult to process and cannot easily be integrated with silicon technologies.<sup>2,3</sup> Guest-host poled polymers are an alternative to inorganic crystals; however, their NLO behavior is somewhat unstable,<sup>4,5</sup> especially at high temperatures.

Alternatively, ionically self-assembled monolayers (ISAMs) are inexpensively fabricated and offer temporally and thermally stable nonlinear optical properties without the need of poling.<sup>6</sup> The synthesis of ISAMs is based on the successive electrostatic buildup of oppositely charged monolayers. A negatively charged substrate is first dipped

into an aqueous polycation solution. The polycations electrostatically bind to the negatively charged substrate, resulting in a charge reversal of the surface. The positively charged substrate is then dipped into a polyanion solution that will bind to the previously deposited polycation monolayer, reverting back to a negatively charged surface (Fig. 1). This assembly process is easily scaled and automated.

The inherent low cost of “soft” patterning techniques such as nanoimprint lithography (NIL) offers a commercially viable pathway for the manufacturing of photonic and electronic devices requiring nanometer-scale feature sizes.<sup>7</sup> Nanoimprint lithography consists of molding a thermoplastic polymer with a master by applying a constant force at a temperature exceeding its glass transition temperature. Under these conditions, the polymer flows and conformably contacts the master. Demolding is performed once the system temperature is lowered, resulting in a topography of the imprinted polymer that is the negative image of the master. Nanometer-scale feature sizes are readily achieved because this technique is not limited by diffraction or scattering phenomena. In addition, NIL is not prone to overetching problems encountered with wet etching.<sup>8,9</sup> The technique is therefore readily conducive to the patterning of features of <10 nm.<sup>8</sup> In addition, typical dry etching methods employed in microfabrication induce some level of surface roughness that generates scattering losses.<sup>7</sup> Nanoimprint lithography may reduce these losses by allowing the fabrication of vertical structures with smoother side-

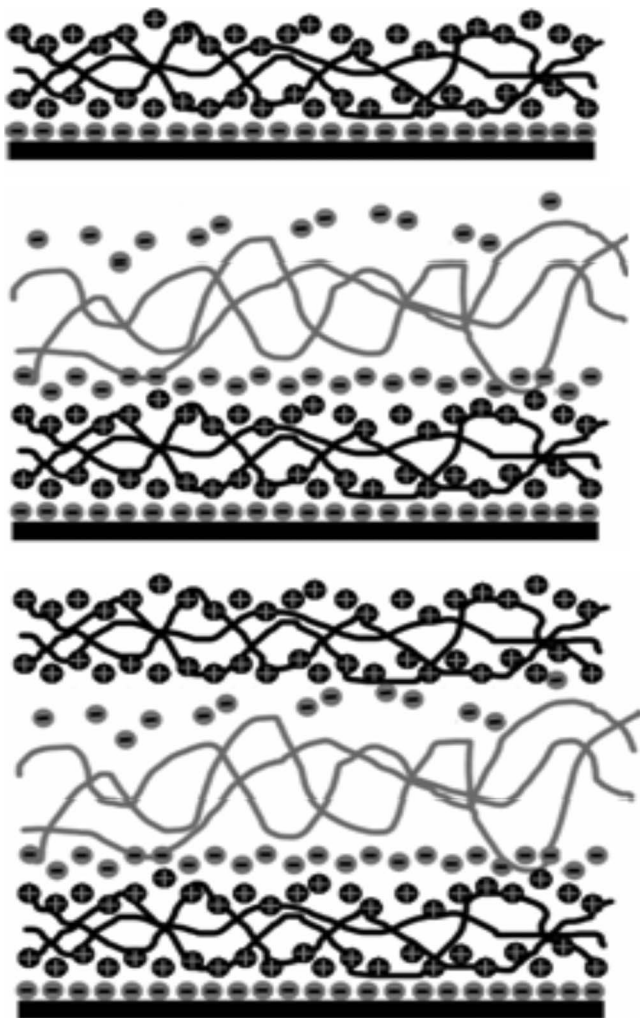


**Fig. 1** Ionically self-assembled monolayer deposition technique. A negatively charged substrate is alternatively dipped in polycation and polyanion solutions, electrostatically building up oppositely charged monolayers.

walls. Photonic structures such as microring resonators<sup>7</sup> and photonic crystal structures<sup>9,10</sup> have already been realized using NIL.

Poled polymers are not easily compatible with nanoimprinting and require an additional poling step during heating to ensure NLO behavior. In contrast, ISAM films are compatible to the thermal cycles associated with nanoimprinting, enabling a platform for the cost-effective mass manufacturing of nonlinear devices in organic materials.

We report such development of both reactive ion etch and nanoimprint lithography-based fabrication methodologies that uses ISAM films as a materials platform for photonic structures. A review of organic nonlinear materials is first presented, followed by the experimental details of ISAM film synthesis and patterning. Results demonstrating both ISAM films' suitability to the nanoimprinting process and the fabrication of photonic devices in such materials are then discussed.

## 2 Overview of Organic Nonlinear Materials

Multiple techniques have been reported to synthesize organic films featuring a NLO effect. Such materials include

poled polymers, Langmuir–Blodgett (LB) films, covalent self-assembled monolayer (CSAM) films, and ISAM films.

Poled polymers are the most common because they are rapidly and easily deposited, with the poling process usually being the most time-consuming step.<sup>4</sup> These materials consist of a host polymer material that is doped with NLO chromophore guests.<sup>3</sup> The doped polymers are not NLO active as-deposited due to the random alignment of their chromophores. Such poling will be induced by application of an electric field that will impart the noncentrosymmetric chromophore alignment necessary for NLO activity. Unfortunately, the chromophore alignment is somewhat unstable<sup>4,5</sup> and will eventually relax even at room temperature.<sup>2</sup> This polar stability decreases even more at high temperatures, rendering them impractical for applications and processes involving elevated temperatures.<sup>3,11,12</sup> Introduction of chromophores into a polymer will also decrease its glass transition temperature,<sup>4</sup> which should be as high as possible for the reasons outlined above. In addition, because the polymers are not bound to any molecules, chromophores have been reported to diffuse to the surface and evaporate or sublime at higher temperatures.<sup>4</sup> The resulting nonuniform distribution results in increased scattering of guided light.<sup>4</sup> Covalent bonding of the chromophores to the polymer backbone<sup>2,4</sup> and cross-linking the polymers after poling,<sup>2,13,14</sup> have been shown to reduce the decay of chromophore alignment.

LB films are synthesized using a layer-by-layer film deposition technique that relies on hydrophilic and hydrophobic interactions.<sup>3</sup> This technique represents a promising alternative to create NLO films because the chromophore alignment is now inherent to the assembly process.<sup>12</sup> Although high electro-optic coefficients have been realized, LB films still display undesirable attributes. The deposition is time consuming,<sup>3,12</sup> expensive,<sup>12</sup> and requires special equipment<sup>15,16</sup> to control the surface pressure.<sup>14,17</sup> If the condensed material aggregates before deposition, then this defect will transfer to the substrate<sup>15</sup> and persist throughout the deposition.<sup>16,18,19</sup> These LB films also possess poor temporal and thermal stabilities.<sup>11,16,17,19,20</sup> Increased stability has, however, been demonstrated with cadmium arachidate by controlling the phase of the deposited monolayer.<sup>19</sup> Another limiting factor is the narrow range of materials that can be deposited because the system must be able to form a monolayer on the surface.<sup>17,20</sup>

CSAM films are more stable<sup>21</sup> due to the involvement of covalent bonds rather than hydrogen bonds. A monolayer is spontaneously formed on a substrate and then chemically activated so another monolayer can covalently attach to it.<sup>3,22,23</sup> The deposition process is also time consuming,<sup>11,18,24</sup> because it requires activation steps for the deposition.<sup>18</sup> The films require 100% reaction yield to prevent nucleation and propagation of defects, rendering the synthesis of thick films difficult.<sup>16,18</sup> Finally, films formed at high temperatures<sup>11</sup> may not be suitable for integration with integrated circuit (IC) technology.

In comparison, ionically self-assembled monolayer films are created with uncomplicated equipment,<sup>25,26</sup> with bilayer formation times on the order of minutes,<sup>3,27</sup> and with an inherent NLO stability that does not involve poling.<sup>3,25,28,29</sup> In addition, deposition is performed at room temperature and is easily automated and scalable with no limit on sub-

strate size. Finally, unlike LB and CSAM films,<sup>18,19</sup> nucleation of defects in the film will not propagate throughout the deposition.<sup>30,31</sup> The NLO-active polyelectrolyte contains chromophores on its side chains that result in a non-centrosymmetric material system that is necessary to present second-order nonlinear behavior.<sup>27</sup> This chromophore orientation is both thermally and thermodynamically stable.<sup>32</sup> Measurements of the second-order susceptibility have demonstrated stability over a period of three years.<sup>32</sup> At higher temperatures, chromophore alignment was maintained in poly S-119/PAH ISAM films.<sup>12</sup> Although the intensity of the second harmonic-generated signal decreased by ~20% at 150 °C, this signal fully reverted to its original value on cooling. This indicates that thermal cycles do not result in a permanent chromophore misalignment demonstrating that ISAM films are fully suitable for nanoimprint lithography

Earlier efforts found poly[1-4-(3-carboxy-4-hydroxyphenylazo) benzenesulfonamido]-1,2-ethanediyl, sodium salt] (PCBS)/poly(allylamine hydrochloride) (PAH) films exhibited an  $r_{33}$  coefficient ranging between 1 and 2 pm/V, which is less than lithium niobate with an  $r_{33}$  coefficient of 32 pm/V. When ISAM films are deposited, the chromophores near the interfaces are oriented both toward and away from the substrate due to their binding to the PAH layers above and below them, resulting in a competitive chromophore alignment that reduces the overall second-order susceptibility.<sup>12,27,33,34</sup> Chromophores in the bulk of the monolayers (not at the interfaces) possess random orientations; thus again, there is a high degree of cancellation.<sup>33,34</sup> More recent hybrid covalent/ionic self-assembly methods using Procion Brown has resulted in films showing  $r_{33}$  coefficients as high as 20 pm/V,<sup>27</sup> roughly two-thirds that of lithium niobate.<sup>4</sup> This method is based on the ionic bonding of the polyanion to the substrate, followed by the directional covalent bonding of a monomeric NLO chromophores to the polyanion layer.<sup>6,11,34</sup> This structure results in higher NLO behavior as the competitive dipole alignment and random orientation in the bulk are eliminated, resulting in a high degree of chromophore order.<sup>6,11,34</sup>

Many methods have been developed to pattern ISAM films. One general approach is to treat ISAM films like conventional photoresists by leveraging polyelectrolytes that chemically react under ultraviolet irradiation. This will induce the formation of bonds between the monolayers that are less soluble in certain solvents.<sup>35-37</sup> Although promising, this method is limited to materials that can react in such a manner. Alternatively, creating surface relief gratings in ISAM films on exposure to linearly polarized light has also been reported.<sup>35,38</sup> The approach is however limited to the patterning of the film surface. Sculptured ISAM films also present a novel patterning method.<sup>39</sup> This technique is, however, restricted to applications desiring membranelike structures. ISAM structures have also been realized using liftoff techniques. A photoresist is first patterned with standard lithography, and ISAM films are then grown over the patterns. Biologically active ISAM testing array<sup>40</sup> and ISAM cantilevers<sup>41</sup> were realized with this liftoff technique. More recently, a soft microstamping technique was also used to pattern ISAM films.<sup>42</sup> In this approach, ISAM materials were first adsorbed onto the patterned surface of a

**Table 1** Chemicals used to synthesize and pattern PCBS/PAH ISAM films with RIE and NIL.

Material	Manufacturer
PCBS	Aldrich
PAH	Aldrich
PMMA 950k A2	MicroChem
HPR 504	Fujifilm
Microposit 354 Developer	Shipley
MIBK:IPA 1:3	MicroChem
Chrome Etch; Semi Grade	Fujifilm
EL	MicroChem
Acetone	J.T. Baker
Isopropyl Alcohol	J.T. Baker
Sulfuric Acid	J.T. Baker
Hydrogen Peroxide	J.T. Baker
Trichloro (1H, 1H, 2H, 2H-perfluorooctyl)-silane	Aldrich
Red Hi-Temp Silicone	Permatex

poly(dimethylsiloxane) stamp and then transferred onto a surface by stamping. Feature size was limited by the stamp size and the ability to grow and transfer films as the stamp critical dimensions decrease or as the film thickness increases. This work focuses on an alternate soft approach to the patterning of ISAMs that rather relies on imprinting of the films, rather than their stamping.

### 3 Experimental Details

#### 3.1 ISAM Film Synthesis and Characterization

Table 1 provides an overview of the materials used to fabricate photonic structures in ISAM films and their manufacturers. The ISAM films were grown both on glass slides (Fisher Scientific) and prime silicon wafers (Silicon Valley Microelectronics, Inc). A 590-nm-thick oxide layer was, however, thermally grown on the silicon wafers using a Minibrute Single Stack oven. This allows working with a starting surface similar to the glass slides typically employed for ISAM synthesis. The substrates were chemically treated in a piranha solution consisting of a 2:1 solution of  $H_2SO_4:H_2O_2$  for 15 min. The piranha removed organic contaminants while inducing a negative surface charge on the substrate via a hydroxylation process.

The NLO-active polyanion, PCBS, was used in conjunction with the NLO-inactive polycation, PAH, for the synthesis of the ISAM films. The average molecular weight of PCBS is 369 g/mol while the one of PAH is 90 g/mol. Both polyelectrolytes were dissolved in deionized (DI) water to create 10-mM solutions. The pH of both solutions

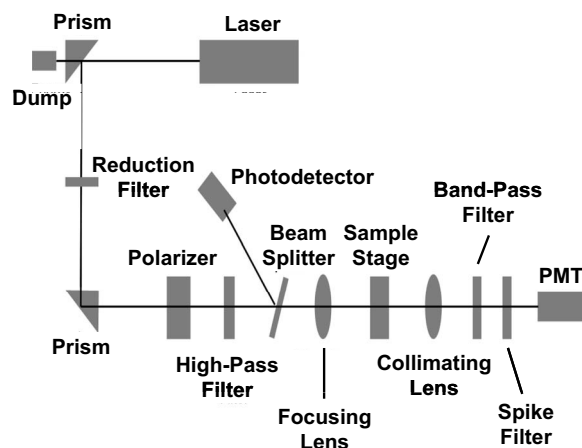


Fig. 2 Schematic diagram of the SHG measurement apparatus.

was adjusted to 7 by adding NaOH and HCl, in order to ensure the consistency of the thickness of each deposited monolayer.

Films were synthesized at room temperature using a Richard-Allen Scientific DS/50 automated slide stainer. The anionic substrates were dipped in the 10-mM cationic PAH solution for 3 min and then rinsed in DI water for 2 min. The now cationic surface was then dipped in the 10-mM anionic PCBS solution for 3 min, followed by another 2-min rinse in DI water. The DI water was continuously replenished and agitated in order to remove excess polyelectrolytes and prevent cross contamination. The solutions were refreshed every 12 h. The deposition always ended with a PCBS layer in order to ensure an optimal nonlinear susceptibility.<sup>27</sup>

The morphology of the PCBS/PAH ISAM films were assessed using a DI-3100 atomic force microscope (AFM) operated in tapping mode, as well as with a Hitachi S4800 high-resolution scanning electron microscope (SEM). The chemical composition and bonding of the PCBS/PAH films was evaluated with a Nicolet 8700 FT-IR Spectrometer for Fourier transform infrared spectroscopy (FTIR) and a Kratos Axis 165 x-ray photoelectron spectrometer (XPS).

Second harmonic generation (SHG) was measured using a Q-switched Nd:YAG pulsed laser (Spectra Physics Quanta-Ray GCR 130) at  $\lambda=1064$  nm (Fig. 2). The pulse frequency was  $f=10$  kHz, and the pulse width was  $\tau=15$  ns at an energy of  $E=500$  mJ. The beam encountered a first prism, in which over 95% of the pulse energy was removed. The remaining reflected beam was further attenuated using filters and then polarized. A high-pass filter prevented any light with a wavelength of  $>700$  nm from being transmitted, therefore eliminating any SHG produced from the optical elements themselves. The beam was then split in two toward a photodetector that recorded the reference beam and toward a lens that focused it onto the sample. The sample was mounted on a stage controlled by stepper motors. After transmission, the beam was collimated and then transmitted through a band-pass filter (between 380 and 600 nm), which filtered out the 1064-nm component of the beam. The final spike filter, at 532 nm, ensured that the only light from SHG was collected by the photomultiplier tube.

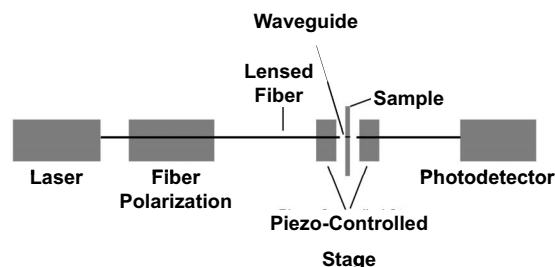


Fig. 3 Optical test apparatus for guiding light in ISAM waveguides.

The light of a tunable laser (Santec TSL-210V) with a wavelength ranging between  $\lambda=1510$  and 1630 nm was guided through a polarization-controlled lensed fiber to perform transmission measurements (Fig. 3). A piezoelectric stage was used to align the tip of the fibers with the fabricated waveguide. An InGaAs photodetector then collected the transmitted light.

### 3.2 Patterning of ISAM Films by Reactive Ion Etching

The process flow used to pattern ISAM films is shown in Fig. 4. The ISAM films were prebaked on a hot plate at  $180^\circ\text{C}$  for 1 h [Fig. 4(a)] to remove residual water resultant from the aqueous nature of monolayer growth. A 580-nm-thick protective HPR 504:ethyl lactate (EL) 5:7 layer was spun on the substrates with a spread cycle for 5 s at 100 rpm and a spin cycle for 30 s at 4000 rpm [Fig. 4(b)] to prevent contact with chrome etch, which attacks the PCBS/PAH ISAM films. The substrate was then baked at  $180^\circ\text{C}$  to drive off residual solvents before a 35-nm low-stress chrome layer was sputtered with a Lesker Magnetron Sputtering System operating at a pressure of

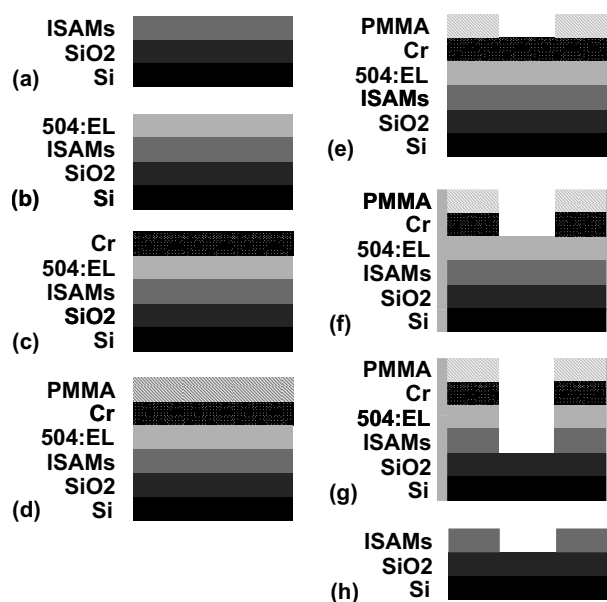


Fig. 4 Process flow depicting the fabrication of photonic structures in ISAM films using EBL and RIE.



Fig. 5 Process flow illustrating the creation of silicon masters.

2.5 mTorr and a power of 300 W [Fig. 4(c)]. This chrome layer masked areas of the ISAM films during the subsequent oxygen plasma.

PMMA 950k electron beam lithography (EBL) resist was then spun [Fig. 4(d)] on the chrome masking layer and exposed [Fig. 4(e)]. Spin parameters for PMMA 950k consisted of a spread cycle for 5 s at 100 rpm and a spin cycle for 30 s at 4000 rpm. The substrates were then baked at 180°C. This process resulted in a PMMA thickness of 120 nm. Typical Raith 150 EBL exposure parameters were an accelerating voltage of 2 keV, a 10- $\mu$ m aperture, and a 15-pA beam current. Following exposure, the PMMA was developed in an MIBK:IPA 1:3 solution for 30 s, placed in a IPA stop bath for 15 s, rinsed in DI water for 15 s, and finally dried with nitrogen. Before the chrome etch step, the sides of the ISAM films were protected with HPR 504:EL 5:7.

The chrome masking layer was etched (f), enabling the HPR 504 and underlying PCBS/PAH ISAM layer to be patterned by the oxygen reactive ion-etching (RIE) plasma in Fig. 4(g). Manual agitation in a chrome etch solution was not sufficient to “wet” some periodic structures because of air-bubble formation. Therefore, chrome was etched using ultrasonic agitation until completion was visible, typically after immersion for 15 s. The TRION Reactive Ion Etch system was used to dry etch the ISAM films. The oxygen plasma was lit with an oxygen flow rate of 15 sccm, a radio frequency (RF) power of 60 W, and a chamber pressure of 5 mTorr. Finally, the protective, HPR 504 and chrome masking layers are removed in an ultrasonic acetone bath leaving patterned ISAM films shown in Fig. 4(h).

### 3.3 Patterning ISAM Films by Nanoimprint Lithography

The process flow for creating silicon masters using in NIL is shown in Fig. 5. EBL was used to create masters in silicon. PMMA 950k resist was spun on the silicon substrates [Fig. 5(a)] and exposed [Fig. 5(b)] with the same parameters presented in Section 3.2. Chrome was deposited using an electron beam evaporation system to a thickness of 30 nm as measured by a crystal thickness monitor [Fig. 5(c)]. Sputtering was not used because of step coverage issues. Liftoff was performed in an ultrasonic acetone bath to remove the resist and overlying chrome layer, resulting in negative-toned chrome patterned silicon [Fig. 5(d)].

The chrome pattern masked the underlying silicon during the silicon etch [Fig. 5(e)]. Deep silicon etching was performed using two different systems, depending on their respective availability. An STS ICPRIE was used at a pressure of 20 mTorr, with a C<sub>4</sub>F<sub>8</sub> flow of 80 sccm and a SF<sub>6</sub>

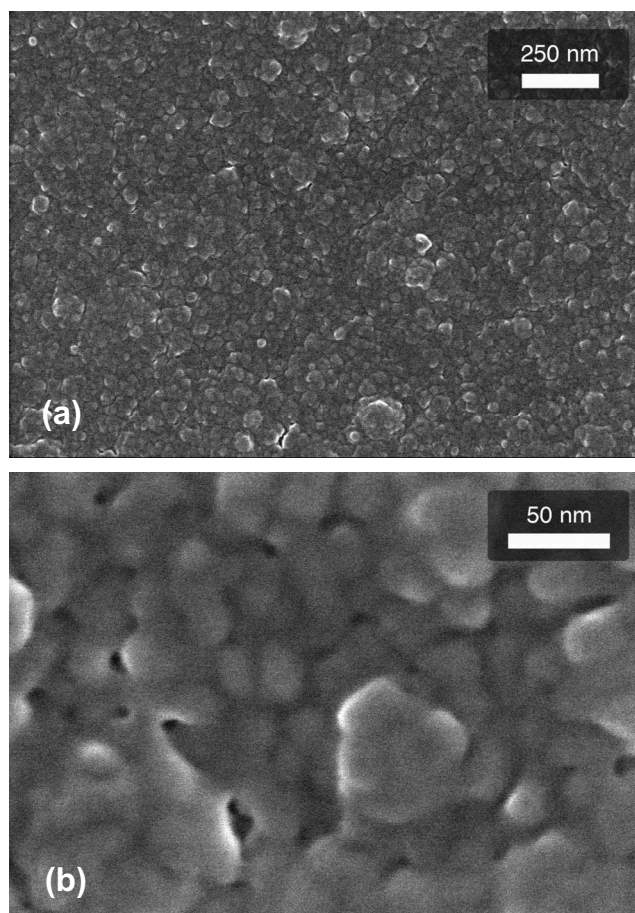
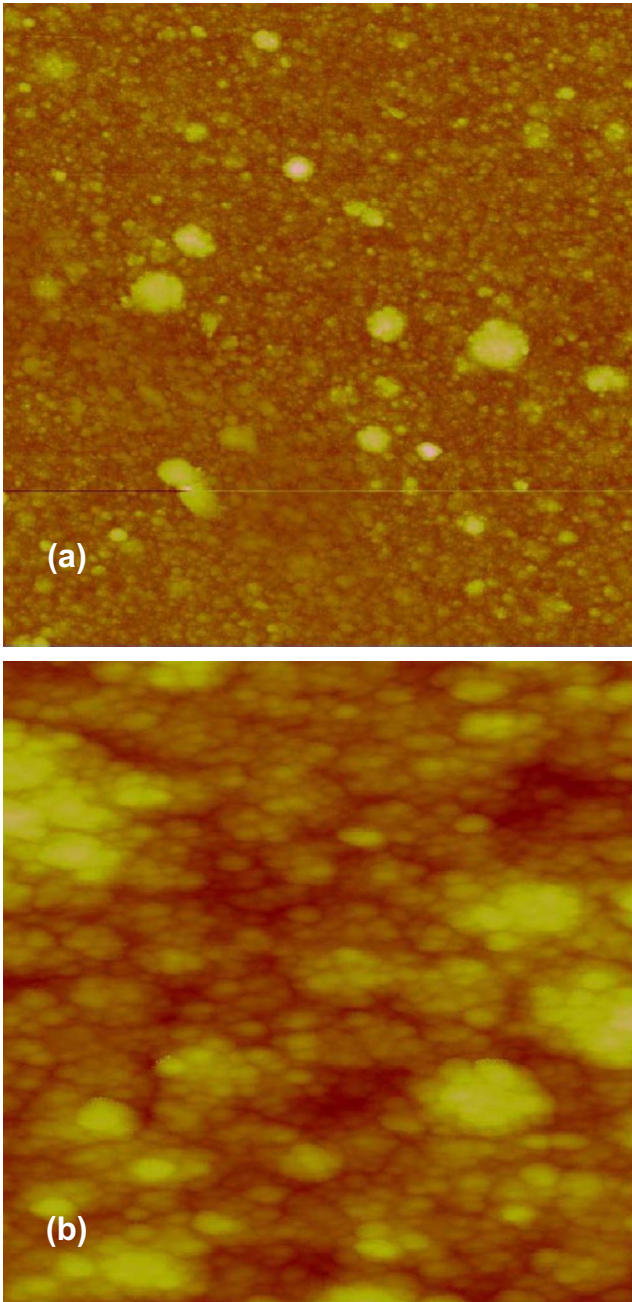


Fig. 6 SEM images of 500 bilayer PCBS/PAH ISAM films are shown in (a) and (b).

flow of 100 sccm. The inductively coupled plasma (ICP) power was 2.5 kW, and the RF power was 20 W. A cryogenic etch was also performed on the Oxford ICPRIE. The exposed silicon was etched with a SF<sub>6</sub> flow of 45 sccm, an O<sub>2</sub> flow of 9 sccm, a pressure of 7.5 mTorr, an ICP power of 400 W, and a RF power of 6 W. After pattern transfer into the silicon, the chrome was removed with the wet chrome etch [Fig. 5(f)]. Finally, to prevent the ISAM films from adhering to the silicon masters, a monolayer of trichloro(1H,1H,2H,2H-perfluorooctyl)-silane was applied to the Si master as an antistiction layer. The silane and master were placed under vacuum for 1 h, resulting in a monolayer of silane forming on the master.

Jenoptik HEX 01 and HEX 02 hot embossing systems were used to imprint the ISAM films. The system consists of two horizontal metal plates whose temperature, position, and force exerted are controlled by manufacturer provided software. All nanoimprinting was performed under vacuum. The glass transition temperature of similar ISAM films was evaluated at 140°C by nanoindentation.<sup>43</sup> These initial studies also indicated that raising the film temperature slightly above their glass transition did not significantly affect their molecular alignment. An imprinting temperature of 145°C was therefore chosen in order to ensure clean molding of the material. The imprinting of the films will also require some displacement of the material. This dis-



**Fig. 7** AFM images of 500 bilayer PCBS/PAH ISAM film with an (a) 10- $\mu\text{m}$  scan size and a (b) 1- $\mu\text{m}$  scan size.

placed material is likely to assume a different molecular alignment than the rest of the film, possibly inhibiting the NLO properties in regions located near the edges of the patterns. As will be discussed below, the imprinted material did retain strong NLO properties even after imprinting, indicating that the thickness of this edge material was not that significant at least for the structure dimensions studied here.

## 4 Results and Discussion

### 4.1 ISAM Film Characterization

The 500 bilayer PCBS/PAH ISAM films are continuous and homogeneous as shown in Figs. 6(a) and 6(b). AFM

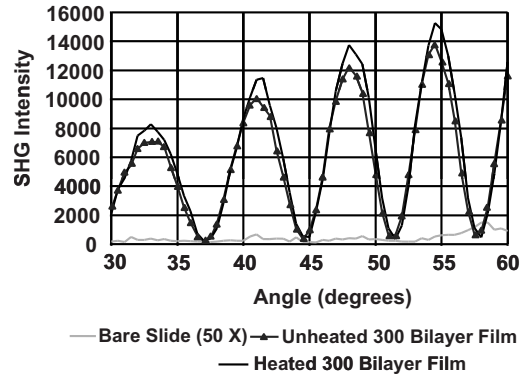


**Fig. 8** Thermal investigation of the SHG of PCBS/PAH ISAM films.

images on the 500 bilayer PCBS/PAH films are shown in Figs. 7(a) and 7(b). The average roughness of these films was 12.4 nm.

The thermal stability and polymeric nature of ISAM films suggest their amenability to NIL for their high-throughput patterning. To that end, the thermal stability of PCBS/PAH films employed here had to be thoroughly examined in order to assess whether the thermal cycling involved in NIL would degrade the chromophore alignment and affect their nonlinear properties.

SHG measurements were taken on PCBS/PAH ISAM films to investigate how heating affected the nonlinear optical properties of the films. The SHG signal was measured on both an unheated film and a film heated for 15 min at  $T=145^\circ\text{C}$  in the hot embossing system that was subsequently used for the imprinting work itself. The similitude between the SHG intensities coming from the two slides (Fig. 8) indicates that the chromophore alignment was not significantly affected by the thermal exposure and is therefore compatible with NIL. A bare slide SHG signal was also measured (and amplified 50 times for visibility in Fig. 8) demonstrating that the SHG signal was resultant from the NLO ISAM films and not substrate itself.

XPS was then employed to verify that the NIL thermal cycling did not affect the chemical composition of the films. To that end, another set of PCBS/PAH ISAM films

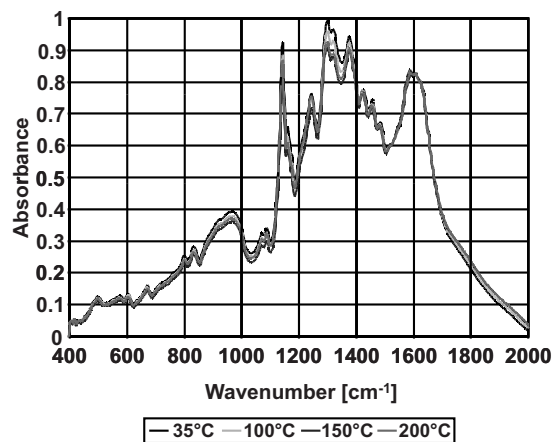


**Fig. 9** FTIR spectra of PCBS/PAH films that have been heated and then cooled back to room temperature.

**Table 2** Percent mass composition of PCBS/PAH ISAM films after being heated to different temperatures and cooled back to room temperature.

Temperature (°C)	Oxygen (%)	Nitrogen (%)	Carbon (%)	Sulfur (%)
35	20.6	12.8	60.0	6.5
100	19.9	13.1	60.5	6.5
150	22.0	10.2	62.2	5.5
200	21.3	11.3	61.7	5.7

were subjected to a 10-min thermal cycle consisting of heating them to temperatures ranging from  $T=35^{\circ}\text{C}$  to  $T=200^{\circ}\text{C}$  for 10 min, and then cooling them back to room temperature. As seen in Table 2, the atomic composition of the PCBS/PAH films was not affected by the heating cycles.

This assessment was further confirmed by FTIR. The similarities between the FTIR spectra after exposure to the 10-min thermal cycles (Fig. 9) further demonstrate that the heating did not alter the chemical bonds within the films. More specifically, the open-chain azo ( $-\text{N}=\text{N}-$ ) feature<sup>44</sup> indicative of the PCBS is seen at  $1600\text{ cm}^{-1}$  and the (C–H) bending indicative of PAH is seen at  $1383\text{ cm}^{-1}$ .<sup>45</sup> Finally, SHG experiments were also performed on fully imprinted films in order to verify that the ISAMs retain their nonlinear properties following actual nanoimprinting. These results are presented further below.

#### 4.2 Patterning ISAM Films by Reactive Ion Etching

For comparison to NIL, a RIE technique was first used to pattern the PCBS/PAH ISAM films because a standard wet chemical etch was not known for such materials and because this dry etch technique could eventually be easily adapted to other types of ISAM films. A  $3\text{-}\mu\text{m}$ -wide waveguide with  $4\text{ }\mu\text{m}$  of air cladding on either side was fabricated using this process in 400 bilayer PCBS/PAH ISAM films [Fig. 10(a)]. Figure 10(b) shows a side view of the resulting oxygen plasma etch profile. The plasma successfully etched through both the HPR 504 protective layer (lighter polymer above) as well as the ISAM films (darker polymer below). Although the etch is very anisotropic, the morphology of the resulting sidewalls is rougher than desirable. This roughness can be attributed to the raggedness of the etched chrome. Finally, hexagonal photonic crystal structures with a lattice spacing of  $710\text{ nm}$  and hole diameters ranging between  $550$  and  $650\text{ nm}$  were also successfully realized [Fig. 10(c)].

#### 4.3 Patterning ISAM Films Using Nanoimprint Lithography

A suitable master had to be fabricated in order to similarly pattern the ISAM films by nanoimprinting. Silicon was selected due to its ease of processing and access to established processes for its machining. Although not as resistant

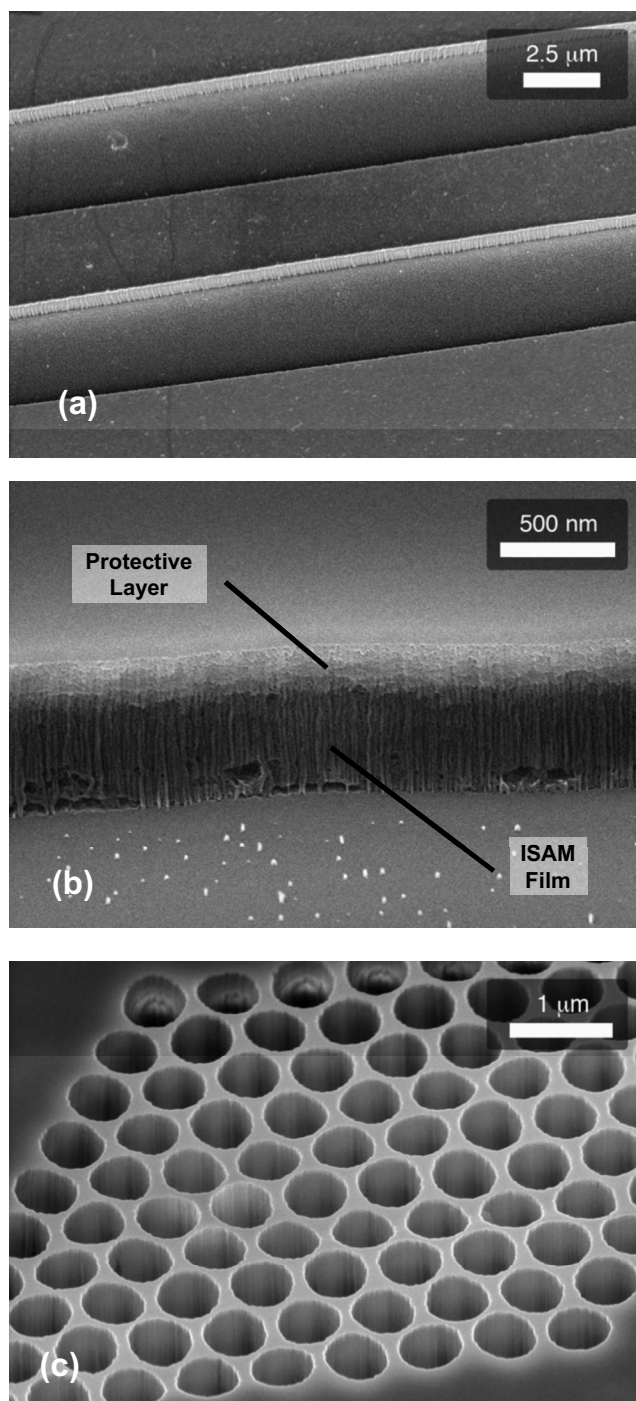


**Fig. 10** PCBS/PAH ISAM films patterned with RIE (a) A waveguide, (b) the sideview of that waveguide, and (c) a photonic crystal structure were fabricated in PCBS/PAH ISAM films using EBL.

to wear as nickel, for instance, silicon is significantly cheaper and therefore enables more flexibility in terms of design modification.

Figure 11(a) shows the silicon master used to create a  $3\text{-}\mu\text{m}$ -wide waveguide with a  $590\text{-nm}$  period Bragg grating. The etching process resulted in a very uniform anisotropic array with no apparent underetching. EBL was also used to fabricate  $490\text{-nm}$ -diam pillars [Fig. 11(b)].

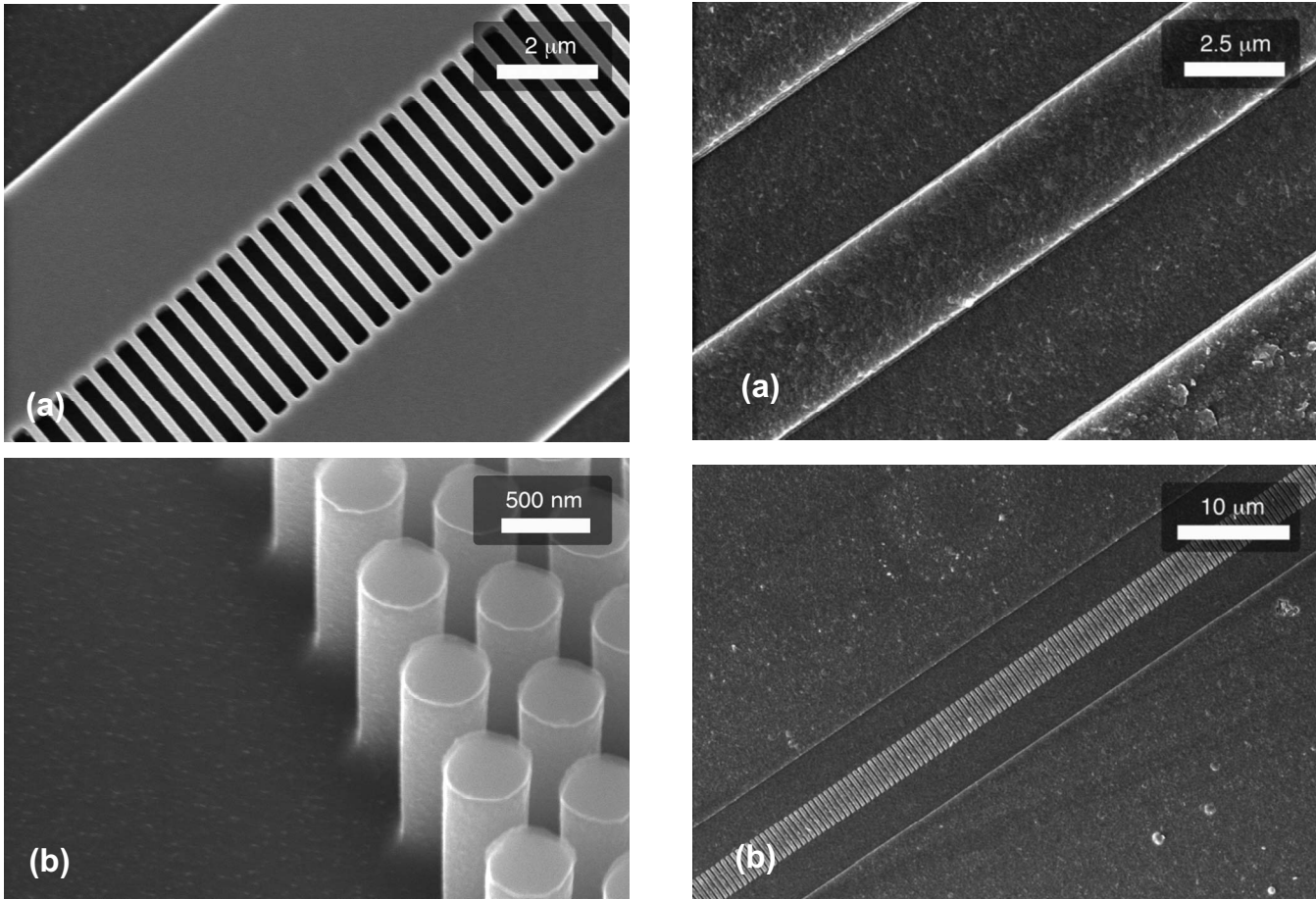


**Fig. 11** Silicon masters of an (a) 3- $\mu\text{m}$  waveguide with a 590-nm period Bragg grating and (b) 490-nm-diam pillars are shown.

Figure 12(a) shows a 3- $\mu\text{m}$ -wide waveguide structure successfully imprinted into an ISAM film. A 3- $\mu\text{m}$ -wide waveguide with an integrated 620-nm period Bragg grating is also shown in Fig. 12(b). Finally, in Fig. 12(c), a hexagonal photonic crystal structure with an average hole diameter of 490 nm and a lattice spacing of 750 nm is shown imprinted in the ISAM film.

The SHG, XPS, and FTIR analysis presented previously indicated that the thermal cycles associated with NIL did not affect the composition of the PCBS/PAH ISAM films. This assessment was further confirmed by performing SHG measurements on actual imprinted patterns in order to verify that the nonlinear properties of the films were still unaffected by overall process. To that end, ISAM films were imprinted for a period of 2 h at 150°C and a pressure of 10 kN with masters with fill factors ranging from 0 to 25%. The films exhibit similar SHG results after nanoimprinting (Fig. 13), indicating again that the NIL process was not affecting the nonlinear optical response of the material.

As discussed in Section 3, there is a strong possibility that some molecular misalignment of the material located at the very edge may inhibit the nonlinear activity near those edges. The SHG results presented here would indicate that this edge misalignment, although likely, is not significantly affecting the NLO of the structure as whole, at least for the

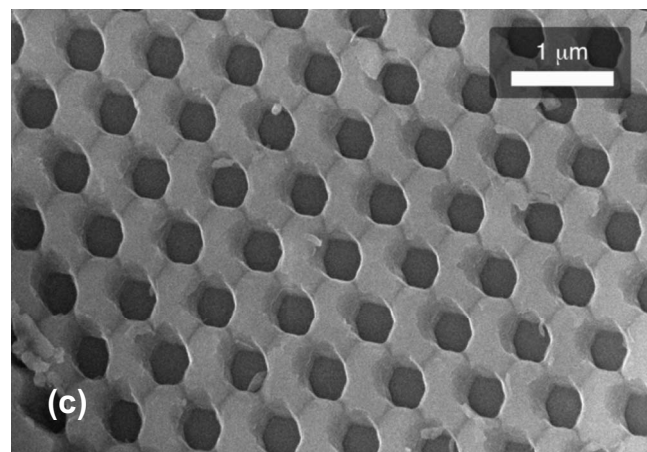


**Fig. 12** (a) 3- $\mu\text{m}$  waveguide structures imprinted into the PCBS/PAH ISAM film is shown (a) and (b) with an integrated 620-nm period Bragg grating as shown. (c) A hexagonal photonic crystal structure with an average hole diameter of 490 nm and a lattice spacing of 750 nm is shown.

dimensions studied here. We would also expect the issue to fully scale for photonic crystals eventually aiming to operate in visible and near-visible range. Indeed, the proportion of the volume to be displaced, and thus, the relative thickness of this edge material would be expected to remain constant as whole design is scaled down.

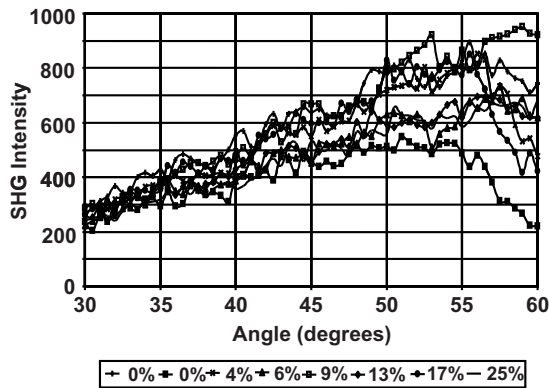


Fig. 13 SHG of PCBS/PAH ISAM films after being imprinted with different area fill factors based on 5- $\mu$ m circles.

#### 4.4 Guiding in ISAM Waveguides

A laser tuned to  $\lambda=1510$  nm was coupled to an ISAM waveguide fabricated by the RIE technique. From an initial 10-mW laser power, guided transmission of 240 nW was observed. Coupling inefficiency does not completely explain this loss. Transmission measurements of silicon waveguides measured on the same setup was found to have powers two to three orders of magnitude higher. The sidewall roughness and the inhomogeneous sites found within the PCBS/PAH ISAM films contribute to this loss via scattering.

A similar assessment was also performed on waveguides that have been fabricated by imprinting rather than by dry etching. In this case, the transmitted power was, however, too low to make a quantitative assessment of the related guiding efficiency. The significant decrease in sidewall roughness that results from eliminating the RIE step should result in a higher transmitted power because of the relatively smooth nanoimprinted walls. As before, the inhomogeneous sites contribute to the loss of transmitted power because they act like scatter sites. As well, the inhomogeneous sites result in incomplete imprinting because more time is needed for sufficient polymer flow. This incomplete imprint reduces the refractive index contrast, making the waveguides more susceptible to scattering losses. Additional work is underway to further refine the morphology of the films, making them fully suitable for optical waveguiding.

## 5 Conclusions

The development of a fabrication platform enabling the use of ISAM films in photonic devices has been reported. More specifically, we have demonstrated the use of NIL to pattern PCBS/PAH ISAM films. Photoelectron and infrared spectroscopy confirmed that the chemical composition of the films was not affected by the heating cycle required by NIL. In addition, measurement of the SHG also confirmed that the NIL process did not affect the alignment of the chromophores responsible for the nonlinear properties of the material. These observations confirm that these materials are suitable to be patterned by nanoimprinting, a key feature that would enable the cost-effective manufacturing of nanophotonic devices leveraging these materials.

PCBS/PAH ISAM films were successfully patterned using both plasma etching and NIL. In the first case, a combination of EBL and RIE was used to machine photonic crystals structures with spacings of 710 nm and hole diameters ranging between 550 and 650 nm. In turn, similar structures were also produced by the direct nanoimprinting of the films. Photonic crystals structures with an average hole diameter of 490 nm and a lattice spacing of 750 nm were successfully imprinted. Bragg gratings with a period of 620 nm were also produced with this method. The inherent nonlinear optical stability of ISAM films, in addition to their ease of processing, is anticipated to enable development of related commercial devices with substantially reduced manufacturing costs.

#### Acknowledgments

This work was funded by the US Air Force Office of Scientific Research (AFOSR) through the SBIR/STTR program. A.K. and S.B. acknowledge financial assistance from the National Sciences and Engineering Scientific Council of Canada through its Industrial Postgraduate Scholarships program. The University of Alberta's NanoFab was utilized to fabricate the photonic structures. SEM was performed at the electron microscopy facilities of the National Institute for Nanotechnology, a joint venture between the National Research Council of Canada, the Province of Alberta, and the University of Alberta. The authors acknowledge Luc Gervais for his assistance with AFM analysis and Neal Wilding for FTIR training.

#### References

1. W. Jiang, Y. Jiang, L. Gu, L. Wang, X. Chen, and R. T. Chen, "Silicon and polymer nanophotonic devices based on photonic crystals," *Proc. SPIE* **6124**, 612410 (2006).
2. M. Eich, G. C. Bjorklund, and D. Y. Yoon, "Poled Amorphous Polymers for Second-Order Nonlinear Optics," *Polym. Adv. Technol.* **1**, 189–198 (1990).
3. X. Cheng and L. J. Guo, "Electrostatic self assembly of nanocomposite polymers in grating Structures," *J. Vac. Sci. Technol. B* **19**(6), 2736–2740 (2001).
4. S. K. Yesodha, C. K. Sadashiva Pillai, and N. Tsutsumi, "Stable polymeric materials for nonlinear optics: a review based on azobenzene systems," *Prog. Colloid Polym. Sci.* **29**, 45–74 (2004).
5. H. Kimura-Suda, Y. Zhang, T. Sassa, T. Wada, and H. Sasabe, "Polar alignment in spin-coated carbazole main- and side-chain polymer films," *Adv. Mater. Res.* **12**(16), 1196–1199 (2000).
6. J. R. Heflin, M. T. Guzy, P. J. Neyman, K. J. Gaskins, C. Brands, Z. Wang, H. W. Gibson, R. M. Davis, and K. E. Van Cott, "Efficient, thermally stable, second order nonlinear optical response in organic hybrid covalent/ionic self-assembled films," *Langmuir* **22**, 5723–5727 (2006).
7. H. Schiff, S. Park, B. Jung, C. Choi, C. Kee, S. Han, K. Yoon, and J. Gobrecht, "Fabrication of polymer photonic crystals using nanoimprint lithography," *Nanotechnology* **16**, S261–S265 (2005).
8. Y. Chou, P. R. Krauss, W. Zhang, L. J. Guo, and L. Zhuang, "Sub-10 nm imprint lithography and applications," *J. Vac. Sci. Technol. B* **15**(6), 2897–2904 (1997).
9. L. J. Guo, "Recent progress in nanoimprint technology and its applications," *J. Phys. D* **37**, R123–R141 (2004).
10. C. Chao and L. J. Guo, "Polymer microring resonators fabricated by nanoimprint technique," *J. Vac. Sci. Technol. B* **20**(6), 2862–2866 (2002).
11. K. E. Van Cott, M. Guzy, P. Neyman, C. Brands, J. R. Heflin, H. W. Gibson, and R. M. Davis, "Layer-by-layer deposition and ordering of low-molecular-weight dye molecules for second-order nonlinear optics," *Angew. Chem., Int. Ed.* **41**(17), 3235–3238 (2002).
12. Z. Wang, J. R. Heflin, R. H. Stolen, and S. Ramachandran, "Highly sensitive optical response of optical fiber long period gratings to nanometer-thick ionic self-assembled multilayers," *Appl. Phys. Lett.* **86**, 223104 (2005).

13. R. P. Bertram, N. Benter, D. Apitz, E. Soergel, K. Buse, R. Hagen, and S. G. Kostromine, "Increased thermal stability of a poled electro-optic polymer using high-molar-mass fractions," *Phys. Rev. E* **70**, 041802 (2004).
14. C. Figura, P. Neyman, D. Marciu, C. Brands, M. A. Murray, S. Hair, R. M. Davis, M. B. Miller, and J. R. Heflin, "Thermal stability and immersion solution dependence of second order nonlinear optical ionically self-assembled films," *Proc. SPIE* **3939**, 214–222 (2000).
15. G. G. Roberts, "An applied science perspective of Langmuir-Blodgett films," *Adv. Phys.* **34**(4), 475–512 (1985).
16. G. Decher, "Fuzzy nanoassemblies: toward layered polymeric multicomposites," *Science* **277**, 1232–1237 (1997).
17. J. A. Zasadzinski, R. Viswanthan, L. Madsen, J. Garnaes, and D. K. Schwartz, "Langmuir-Blodgett films," *Science* **263**(5154), 1726–1733 (1994).
18. Y. Liu, A. Rosidian, K. Lenahan, Y. Wang, T. Zeng, and R. O. Claus, "Characterization of electrostatically self-assembled nanocomposite thin films," *Smart Mater. Struct.* **8**, 100–105 (1999).
19. D. Y. Takamoto, E. Aydil, J. A. Zasadzinski, A. T. Ivanova, D. K. Schwartz, T. Yang, and P. S. Cremer, "Stable ordering in Langmuir-Blodgett films," *Science* **293**, 1292–1295 (2001).
20. D. L. Allara, "Critical issues in applications of self-assembled monolayers," *Biosens. Bioelectron.* **10**, 771–783 (1995).
21. R. Paolesse, C. Di Natale, A. Macagnano, F. Davide, T. Boschi, and A. D'Amico, "Self-assembled monolayers of mercaptoporphyrins as sensing material for quartz crystal microbalance chemical sensors," *Sens. Actuators B* **47**, 70–76 (1998).
22. S. Stockhause, P. Neumann, S. Schrader, M. Kant, and L. Brehmer, "Structural and optical properties of self-assembled multilayers based on organic zirconium bisphosphonates," *Synth. Met.* **127**(1–3), 295–298 (2002).
23. W. Lin, W. Lin, G. K. Wong, and T. J. Marks, "Supramolecular approaches to second-order nonlinear optical materials. self-assembly and microstructural characterization of intrinsically acentric [(aminophenyl)azoa]pyridinium superlattices," *J. Am. Chem. Soc.* **118**, 8034–8042 (1996).
24. T. Wink, S. J. van Zuilen, A. Bult, and W. P. van Bennekom, "Self-assembled monolayers for biosensors," *Analyst (Amsterdam)* **122**, 43R–50R (1997).
25. J. R. Heflin, Y. Liu, C. Figura, D. Marciu, and R. O. Claus, "Second order nonlinear optical thin films fabricated from ionically self-assembled monolayers," *Proc. SPIE* **3147**, 10–19 (1998).
26. A. Rosidian, Y. Liu, and R. O. Claus, "Ionic self-assembly of ultrahard ZrO<sub>2</sub>/polymer nanocomposite thin films," *Adv. Mater. Res.* **10**(14), 1087–1091 (1998).
27. J. R. Heflin, C. Durak, P. J. Neyman, C. Brands, M. T. Guzy, K. Gaskins, A. Garg, R. M. Davis, K. E. Van Cott, H. Wang, and H. W. Gibson, "Organic electro-optic films fabricated by hybrid covalent/ionic self-assembly," *Conference on Lasers & Electro-Optics* **3**, 1864–1866 (2005).
28. G. Purvinis, P. S. Priambodo, M. Pomerantz, M. Zhou, T. A. Maldonado, and R. Magnusson, "Second-harmonic generation in resonant waveguide gratings incorporating ionic self-assembled monolayer polymer films," *Opt. Lett.* **29**(10), 1108–1110 (2004).
29. F. J. Arregui, B. Dickerson, R. O. Claus, I. R. Matias, and K. L. Cooper, "Polymeric thin films of controlled complex refractive index formed by the electrostatic self-assembled monolayer process," *IEEE Photonics Technol. Lett.* **13**(12), 1319–1321 (2001).
30. F. J. Arregui, I. R. Matias, K. L. Cooper, and R. O. Claus, "Fabrication of microgratings on the ends of standard optical fibers by the electrostatic self-assembly monolayer process," *Opt. Lett.* **26**(3), 131–133 (2001).
31. K. Hyde, M. Rusa, and J. Hinestroza, "Layer-by-layer deposition of polyelectrolyte nanolayers on natural fibres: cotton," *Nanotechnology* **16**, S422–S428 (2005).
32. J. R. Heflin, C. Figura, D. Marciu, Y. Liu, and R. O. Claus, "Thickness dependence of second-harmonic generation in thin films fabricated from ionically self-assembled monolayers," *Appl. Phys. Lett.* **74**(4), 495–497 (1999).
33. D. A. Chang-Yen and B. K. Gale, "An integrated optical biochemical sensor fabricated using rapid-prototyping techniques," *Lab Chip* **3**, 297–301 (2003).
34. P. J. Neyman, M. Guzy, S. M. Shah, R. M. Davis, K. E. Van Cott, H. Wang, H. W. Gibson, C. Brands, and J. R. Heflin, "Novel hybrid covalent/ionic self-assembly technique for improved second-order nonlinear optical films," *Mater. Res. Soc. Symp. Proc.* **708**, BB4.4.1–BB4.4.6 (2002).
35. O. N. Oliveira, Jr., D. S. dos Santos, Jr., D. T. Balogh, V. Zucolotto, and C. R. Mendonca, "Optical storage and surface-relief gratings in azobenzene-containing nanostructured films," *Adv. Colloid Interface Sci.* **116**, 179–192 (2005).
36. P. Bertrand, A. Jonas, A. Laschewsky, and R. Legras, "Ultrathin polymer coatings by complexation of polyelectrolytes at interfaces: suitable materials, structure and properties," *Macromol. Rapid Commun.* **21**, 319–348 (2000).
37. T. Cao, F. Wei, X. Jiao, J. Chen, W. Liao, X. Zhao, and W. Cao, "Micropatterns of protein and conducting polymer molecules fabricated by layer-by-layer self-assembly and photolithography techniques," *Langmuir* **19**, 8127–8129 (2003).
38. C. S. Camilo, D. S. dos Santos, Jr., J. R. Rodrigues, Jr., M. L. Vega, S. P. Campana Filho, O. N. Oliveira, Jr., and C. R. Mendonça, "Surface-relief gratings and photoinduced birefringence in layer-by-layer films of chitosan and an azopolymer," *Biomacromolecules* **4**, 1583–1588 (2003).
39. Y. Lin, C. Jiang, J. Xu, Z. Lin, and V. V. Tsukruk, "Sculptured layer-by-layer films," *Adv. Mater. Res.* **19**, 3827–3832 (2007).
40. D. Wang, A. L. Rogach, and F. Caruso, "Composite photonic crystals from semiconductor nanocrystal/polyelectrolyte-coated colloidal spheres," *Chem. Mater.* **15**, 2724–2729 (2003).
41. D. Kommireddy, J. Shi, X. Yan, H. Ji, and Y. Lvov, "Electrostatic layer-by-layer nano-assembly: films, cantilevers, micropatterns and nanocapsules," *Proc. SPIE* **4492**, 120–131 (2005).
42. J. Park and P. T. Hammond, "Multilayer transfer printing for polyelectrolyte multilayer patterning: direct Transfer of layer-by-layer assembled micropatterned thin films," *Adv. Mater. Res.* **16**(6), 520–525 (2004).
43. C. C. Figura, "Second order nonlinear optics in ionically self-assembled films," PhD Thesis, Virginia Tech (1999).
44. J. Coates, "Interpretation of infrared spectra, a practical approach," *Encyclopedia of Analytical Chemistry*, R. A. Meyers, Ed., pp. 10815–10837, Wiley, Chichester (2000).
45. V. Zucolotto, M. Ferreira, M. R. Cordeiro, C. J. L. Constantino, D. T. Balogh, A. R. Zanatta, W. C. Moreira, and O. N. Oliveira, Jr., "Unusual interactions binding iron tetrasulfonated phthalocyanine and poly(allylamine hydrochloride) in layer-by-layer films," *J. Phys. Chem. B* **107**, 3733–3737 (2003).



**Aruna Kroetch** received her BSc in engineering physics at the University of Alberta in 2003 after which she went on to work at the University of Alberta's Nanofab as a research professional. She completed her MSc in electrical and computer engineering in 2008 at the University of Alberta where the focus of her thesis work was on the fabrication, characterization, and patterning of ISAM films. She is currently working at Miralyn Inc. in the R&D department as a project engineer.



**Steven C. Buswell** received his BSc in engineering physics and MSc in electrical engineering from the University of Alberta in 2005 and 2008, respectively. His thesis research was centered on the design, fabrication, and sensing applications of photonic crystals. He currently is an engineer with Applied Nanotools Inc.



**Stephane Evoy** received his PhD in applied physics from Cornell University in 1998. He is associate professor of electrical and computer engineering at the University of Alberta, with a cross appointment as research officer at the National Institute for Nanotechnology in Edmonton, Alberta. His current research includes the development and integration of nanomechanical devices for biosensing applications and the integration of nanostructures for the development of chemical sensing arrays. Evoy has also recently coedited *Introduction to Nanoscale Science and Engineering*, a textbook supporting the teaching of nanoscale technologies at the undergraduate level. He is currently serving as secretary of the executive committee of the Nanoscale Science and Technology Division of the American Vacuum Society and since 2005 has been a member of the editorial board of *Review of Scientific Instruments*.



**Cemil Durak** received his BS in physics from Bilkent University, Ankara, Turkey, in 2002, and his MS in physics in 2005 from Virginia Tech, Blacksburg, Virginia. He has been doing his graduate studies on second-order nonlinear properties of ionically self-assembled multilayers films under the supervision of Prof. James Heflin. He is planning to finish his doctorate studies on December 2008.



**J. Randy Heflin** is professor of physics and associate director of the Center for Self-Assembled Nanostructures and Devices at Virginia Tech, where he has been a member of the faculty since 1992. He received his PhD from the University of Pennsylvania in 1990. His research focuses on organic optoelectronic nanostructures and devices. He coedited the textbook *Introduction to Nanoscale Science and Technology* (Springer, 2004) and is an associate editor of the

*International Journal of Nanoscience*.



**Vladimir Kochergin** joined the Optical Systems Group at Luna Innovations in September 2006. While at Luna, Vladimir's responsibilities include project and program management. He received his BS and MS in applied physics in 1996 and 1998, respectively, from Moscow Institute of Physics and Technologies, and PhD in materials science in 2007 from Christian Albrecht University of Kiel, Germany. Prior to Luna, he held a similar position in the R&D Department (from 2000 to 2004) and was managing the Optics R&D Department from 2005 to 2006 at Lake Shore Cryotronics, Inc., Columbus, OH. Kochergin has over 50 publications (including a monograph and 11 assigned patents) in the field of photonics, plasmonics, and structural optical materials.



**Roger Duncan** joined the Optical Systems Group of Baker Hughes ProductionQuest in May 2008 as the senior optical systems engineer. While at ProductionQuest, his responsibilities centered on managing the development of the company's OFDR-based distributed fiber-optic sensing platform. Prior to joining ProductionQuest, he served as a senior electro-optic engineer and program manager at Luna Innovations Inc., where he led the distributed fiber-optic

sensing development team and was a primary inventor of the fiber-optic shape-sensing technology. Duncan graduated from Virginia Tech in 2002 with his MS in electrical engineering with an emphasis in electromagnetics and optics. He has authored more than 24 publications related to electro-optics, fiber-optic sensing, and photonic crystals.